Multiscale, thermomechanical topology optimization of self-supporting cellular structures for porous injection molds

Tong Wu[1] **Andres Tovar**[2]

[1] Purdue University, USA, wu616@purdue.edu
[2] Indiana University-Purdue University Indianapolis, Indianapolis, USA, tovara@iupui.edu

Abstract

Purpose – This paper aims to establish a multiscale topology optimization method for the optimal design of non-periodic, self-supporting cellular structures subjected to thermo-mechanical loads. The result is a hierarchically complex design that is thermally efficient, mechanically stable, and suitable for additive manufacturing.

Design/methodology/approach – The proposed method seeks to maximize thermo-mechanical performance at the macroscale in a conceptual design while obtaining maximum shear modulus for each unit cell at the mesoscale. Then the macroscale performance is re-estimated and the mesoscale design is updated until the macroscale performance is satisfied.

Findings – A two dimensional MBB beam withstanding thermo-mechanical load is presented to illustrate the proposed design method. Furthermore, the method is implemented to optimize a three-dimensional injection mold, which is successfully prototyped using 420 stainless steel infiltrated with bronze.

Originality/value – By developing a computationally efficient and manufacturing friendly inverse homogenization approach, the novel multiscale design could generate porous molds which can save up to 30% material compared to their solid counterpart without decreasing thermo-mechanical performance.

Practical implications – This study is a useful tool for the designer in molding industries to reduce the cost of the injection mold and take full advantage of additive manufacturing.

Key words 3D Multiscale topology optimization. Additive Manufacturing. Injection mold.

1. Introduction

Molds used in the plastic injection molding process must withstand extreme pressure loads and thermal expansion, while at the same time providing dimensional accuracy of the molded part. These molds are required to efficiently and uniformly transfer heat flux from the molded part to cooling channels [1]. In conventional molds, the cooling system often consists of straight-line cooling channels, which can be manufactured using machining processes; however, they are thermally inefficient and unable to cool the injected part uniformly. The emergence of metal based Additive Manufacturing (AM) enables the design and production of intricate conformal cooling channels in molds, offering significant cost savings, particularly in designs having high geometric complexity. These AM technologies include Direct Metal Laser Sintering (DMLS), Electron Beam Melting (EBM) and Selective Laser Melting (SLM) [2]. The unique capabilities of AM technologies allow innovative design approachs that challenge traditional guidelines of the several major industries including plastics injection molding [3, 4].

These approaches, aiming to reduce the AM cost without decreasing the performance of design part, can be divided into three groups, namely macroscale (structural) design, mesoscale (meta-material) and multiscale design. In macroscale, structural optimization, including size optimization, shape optimization and topology optimization, are the most commonly used methods for parts design of additive manufacturing . Among them, topology optimization has the best design flexibility since it allows material distributed in terms of physics requirement, offering the potential to create novel and complex parts with high performance and reducing material cost [5, 6]. Some studies have been investigated to develop design frameworks of topology optimization for additive manufacturing for mechanical, thermal and thermo-mechanical structures [5, 7, 8]. In mesoscale, the solid phase meta-materials can be replaced with open cell lattice or porous materials, without changing the macroscale geometry contours [3, 16, 17]. Finally, in a multiscale design, both macroscale and mesoscale design method are simultaneously applied [11, 9, 12, 14, 15]. The most computationally efficient and manufacturing friendly multiscale approach is called Topology Optimization with Functionally Graded Unit Cells [14, 15]. In this method, homogenized properties of a series of pre-defined lattice unit cells with functionally graded relative densities, from void to solid, are derived. The properties of these unit cells are synthesized and implemented in the macroscale topology optimization, leading optimal structures that composed of quasi-periodically distributed,

This is the author's manuscript of the article published in final edited form as:

Wu, T., & Tovar, A. (2018). Multiscale, thermomechanical topology optimization of self-supporting cellular structures for porous injection molds. Rapid Prototyping Journal. https://doi.org/10.1108/RPJ-09-2017-0190

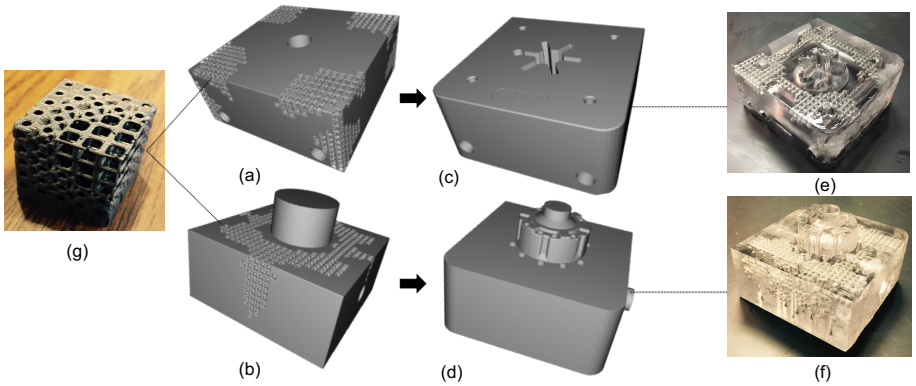

Figure 1: (a) The lattice structure of the design domain of the cavity; (b) The lattice structure of the design domain of the core; (c) The final design of the cavity; (d) The final design of the core; (e) The final 3D-printed cavity in plastic resin; (f) The final 3D-printed core in plastic resin; (g) A lattice structure sample 3D-printed in stainless steel.

functionally graded unit cells. As an example, in our previous work [15], injection molds designed using this method can ideally save 10% to 30% of material cost without compromising thermo-mechanical performance of the mold, as well as maintaining the geometry in contact with other mold assemblies (Fig.1).

Despite of the straightforward of this method, in such optimal design, the geometry complexity of the unit cells are limited since they are controlled by limmited functionally graded parameters. Furthermore, these lattice unit cells may consist of some undesirable long overhanging struts, which lead risks of deformation or sagging in the manufacture process. To support these unstable structures, additional material would be required during AM process. As a result, the actual material usage is more than anticipated. In addition, the removal of large amount of support materials for delicate lattice unit cell structures is time consuming and may breaking off small pieces of lattices. An efficient strategy to reduce support structure materials is to construct self-supporting lattice unit cells in mesoscale design. Self-supporting strucuture ensures that, during the manufacturing process of these cells, one building layer can be supported by its underneath layer without distorted too much or even fail [16]. To obtain a self-supporting lattice structure, the fabrication angle between horizontal plane and downward face of the lattice unit cell should be more than some critical values between 40° to 45° [17]. Typical design strategies to design structures fulfilled this fabrication angle criterion include Computer Aided Design (CAD), biological architecture image data based design, and implicit surface design based on analytical mathematical equations. However, all of these strategies are developed by means of designers' intuition and experience, often requiring a tedious trial and error process to achieve the expected properties. Fortunately, the inverse homogenization method can complement this weakness [18]. With application of inverse homogenization, the optimum topologies of a lattice unit cell with maximum bulk modulus, shear modulus or heat conduction can be obtained [19, 20]. Among these topologies, the lattice unit cell having maximum shear modulus represents a diamond shape that benefit to reduce the support structure material in AM process.

However, inverse homogenization method is mainly implemented in a mesoscale design rather than in a multiscale design, probably due to the high computational cost to optimize each unit cell. In this study, a multiscale thermo-mechanical topology optimization algorithm involved a computationally efficient inverse homogenization method is proposed. A multiscale topology optimization specifies that, the optimized topologies are achieved in both macroscale structure and mesoscale unit cells. The two scales topologies can be optimized either concurrently or hierarchically. The concurrent approach is computationally efficient but it results in only one periodically distributed mesoscale topology [11], while the hierarchically approach can attain optimized properties for each lattice unit cell but it costs significant computational resource and time. Although this hierarchical approach has been an active research topic for many years [9, 12], few of them are applied this approach in three dimensional design with consideration of manufacture issues. In our study, by implementing a computationally efficient inverse homogenization

method to maximize shear modulus of each unit cell, the whole structure is self-supporting and easy to manufacture. Furthermore, a Hybrid Cellular Automata (HCA)[30] updating scheme is employed to guaranteed the thermo-mechanical performance of the macroscale structure. Also, compared to our previous work[15], the method brings a manufacturing friendly design and the design accuracy is improved since each mesoscale unit cell is optimized.

The paper is organized as following: homogenization method, which is the foundation of the proposed approach, will be briefly reviewed in section 2. Then, the proposed multiscale thermo-mechanical topology optimization is presented in section 3. In section 4, the method is demonstrated by optimizing a solid mold to a porous injection mold. In Section 5, the issues with respect to final design, manufacturing as well as future experiment plan are described. Finally, conclusion is presented in section 6.

2. Homogenization method

The material design is formulated as a structural optimization problem and be optimized using inverse homogenization method [21]. The objective function of this method contains effective properties of investigated material, which are found by numerical homogenization. Numerical homogenization can be implemented in asymptotic method (AH), mutual energy approach and represent volume element (RVE)-based approach. All of them can be used to derive homogenized elasticity tensor $\mathbf{D}_c^H$ and thermal conductivity tensor $\boldsymbol{\kappa}_c^H$ of an a-priori defined unit cell. In this section, these methods are briefly reviewed before presenting the proposed multiscale thermomechanical topology optimization approach.

2.1. Asymptotic homogenization

Asymptotic homogenization (AH) assumes each mesoscale unit cell in a macroscale structure follows periodic boundary condition (PBC). The measurable quantity of a unit cell u is the superposition of macroscale quantity $u_0(x, y)$ and a small periodically fluctuated mesoscale quantity $u_1(x, y)$, which can be represented using first order asymptotic expansion:

$$u^\epsilon = u_0(x, y) + \epsilon u_1(x, y) + \mathcal{O}(\epsilon^2), \quad y = x/\epsilon, \quad \epsilon \ll 1. \tag{1}$$

Asymptotic homogenization can be rewritten in an equivalent discretized form in terms of element mutual energies:

$$\mathbf{D}_c^H = \frac{1}{|V_c|} \sum_{e=1}^{n_e} \int_{V_e} [\mathbf{I} - \mathbf{B}_e \boldsymbol{\chi}_e]^\intercal \mathbf{D}_e [\mathbf{I} - \mathbf{B}_e \boldsymbol{\chi}_e] \mathrm{d}V_e, \tag{2}$$

where n_e are the number of finite elements of the discretized unit cell, $|V_c|$ is the unit cell volume, $\mathbf{I}$ is the identity matrix, V_e is the volume of the finite element e, $\mathbf{B}_e$ is the elemental strain-displacement matrix, $\mathbf{D}_e$ is the elemental elasticity tensor, and $\boldsymbol{\chi}_e$ is the matrix containing the element displacement vectors $\boldsymbol{\chi}_e^{ij}$ resulting from globally enforcing the unit test strain fields $\boldsymbol{\varepsilon}^{ij}$ ($[\boldsymbol{\chi}_e^{11}, \boldsymbol{\chi}_e^{22}, \boldsymbol{\chi}_e^{12}]$ for a 2D finite element). The elemental displacement vectors $\boldsymbol{\chi}_e^{ij}$ are obtained from the global displacement vector of the unit cell $\boldsymbol{\chi}_c^{ij}$, which is the solution of the equilibrium equation

$$\left[\sum_{e=1}^{n_e} \int_{V_e} \mathbf{B}_e^\intercal \mathbf{D}_e \mathbf{B}_e \mathrm{d}V_e \right] \boldsymbol{\chi}_c^{ij} = \sum_{e=1}^{n_e} \int_{V_e} \mathbf{B}_e^\intercal \mathbf{D}_e \boldsymbol{\varepsilon}^{ij} \mathrm{d}V_e. \tag{3}$$

The first term in the left hand side of Eq. (3) is the stiffness matrix of the unit cell and the right hand side is the nodal force vector of the unit cell.

In analogy to homogenization theory for elasticity tensor, homogenized thermal conductivity tensor $\boldsymbol{\kappa}_c^H$ of a discretized periodic unit cell is given by

$$\boldsymbol{\kappa}_c^H = \frac{1}{|V_c|} \sum_{e=1}^{n_e} \int_{V_e} [\mathbf{I} - \mathbf{B}_e^t \mathbf{T}_e]^\intercal \boldsymbol{\kappa}_e [\mathbf{I} - \mathbf{B}_e^t \mathbf{T}_e] \mathrm{d}V_e, \tag{4}$$

where n_e are the number of finite elements of the discretized unit cell, $|V_c|$ is the unit cell volume, $\mathbf{I}$ is the identity matrix, V_e is the volume of the finite element, $\mathbf{B}_e^t$ is the elemental (temperature gradient)-temperature matrix, $\boldsymbol{\kappa}_e$ is the element thermal conductivity tensor, and $\mathbf{T}_e$ is the matrix containing the element nodal temperature vectors $\mathbf{T}_e^{ij}$ resulting from globally enforcing the unit test temperature gradient fields ($[\mathbf{T}_e^1, \mathbf{T}_e^2]$ for a 2D solid finite element). As before, the element temperature vectors $\mathbf{T}_e^i$ are

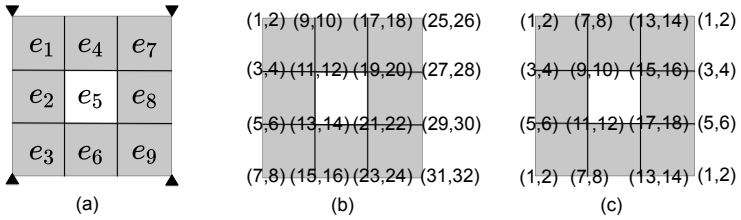

Figure 2: Comparison of Dofs setting between energy-based homogenization and asymptotic homogenization.(a) The discretized unit cell. (b) Dofs used in energy-based homogenization.(c) Dofs used in asymptotic homogenization.

obtained from the global temperature vector of the unit cell $\mathbf{T}_c^i$, which is the solution of the equilibrium equation

$$\left[\sum_{e=1}^{n_e}\int_{V_e}\mathbf{B}_e^{t\intercal}\boldsymbol{\kappa}_e\mathbf{B}_e^t\mathrm{d}V_e\right]\mathbf{T}_c^i=\sum_{e=1}^{n_e}\int_{V_e}\mathbf{B}_e^{t\intercal}\boldsymbol{\kappa}_e\mathbf{t}^i\mathrm{d}V_e. \tag{5}$$

The first term in the left hand side of Eq. (5) is the "stiffness" thermal matrix of the unit cell and the right hand side is the nodal heat flux vector of the unit cell.

2.2. Energy-based homogenization

Energy-based homogenization is an equivalent approach to asymptotic homogenization. In this method, the mutual energy form (Eq. (2) or (4)) and PBC are adopted as well. The difference between these two methods are the implementation of PBC and test strains. In energy-based homogenization, nodal displacement constraints are imposed on each pair of opposites boundaries $k-$ and $k+$ to satisfy PBC:

$$\chi_i^{k+}-\chi_i^{k-}=\varepsilon_0^{ij}\Delta y, \tag{6}$$

where ε_0^{ij} is a given strain and Δy is the length of the unit cell [22]. In asymptotic homogenization, each pair of opposite boundaries share same Dofs (Fig.2) [23], and the test strains are imposed on the whole finite element.

2.3. Representative volume element method

Compared to above two methods, Representative volume element (RVE)-based method is straightforward. It is derived based on the assumption of constant strain fields are uniformly distributed over a RVE, thus homogenized elasticity tensor can be computed by average stress and strain using Hooke's law:

$$\langle\boldsymbol{\sigma}\rangle=\langle\boldsymbol{E}\rangle\langle\boldsymbol{\varepsilon}\rangle, \tag{7}$$

where $\langle\boldsymbol{\sigma}\rangle$ is average stress, and $\langle\boldsymbol{\varepsilon}\rangle$ is average strain of a RVE. In finite element analysis, by applying a group of prescribed unit test strain on the RVE's boundaries, the homogenized properties can be obtained through computation of average stress of the whole element. Using the strain and displacement relations (for 2D problem):

$$\varepsilon_x=\frac{\partial u}{\partial x},\quad \varepsilon_y=\frac{\partial u}{\partial y},\quad \gamma_{xy}=0.5\times(\frac{\partial u}{\partial y}+\frac{\partial v}{\partial x}), \tag{8}$$

applying prescribed displacement $[u=x \quad v=0]$ on RVE's boundary yields an average stresses equal to E_{1111} and E_{2211}, applying prescribed displacement $[u=0 \quad v=y]$ yields average stresses equal to E_{2222} and E_{1122}, and applying prescribed displacement $[u=0.5\times y \quad v=0.5\times x]$ yields E_{1212}.

In analogy to this, homogenized thermal conductivity tensor can be computed by average heat flux and temperature gradient using Fourier's law:

$$\langle\boldsymbol{q}\rangle=\langle\boldsymbol{\kappa}\rangle\langle\nabla\boldsymbol{T}\rangle, \tag{9}$$

where $\langle\boldsymbol{q}\rangle$ is average heat flux. It can be obtained by applying prescribed temperature $T_1=x$ and $T_2=y$ on boundaries.

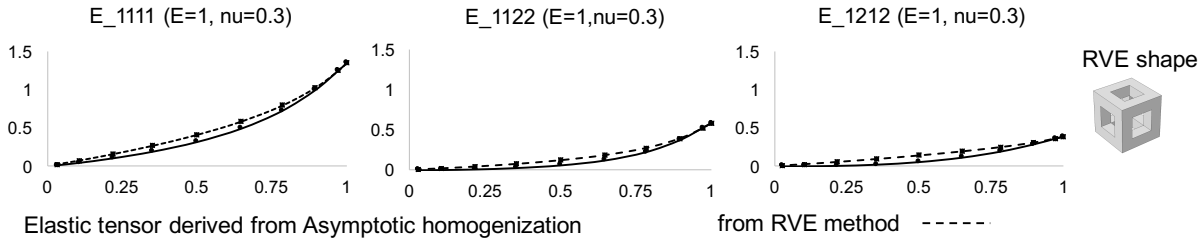

Figure 3: A comparison between RVE-based method and asymptotic homogenization method.

To compare RVE and AH methods, a test using a group of 3D cubes with rectangular holes are implemented as Fig.3 shown. The resulting values from RVE-based method are slightly higher than those derived from AH method and the equivalent energy-based approach, which implies using RVE-based approach may over-evaluate stiffness of the structure. However, RVE-based method has two main advantages over AH method. First, this method is appropriate to evaluate properties of non-periodic mesoscale material, because assumption of periodic boundary condition is not required. In addition, since prescribed displacements on the boundaries are linear functions of geometry coordinate, symmetry condition can be used for finite element analysis, if RVE's center located on the coordinate $(0, 0, 0)$. The computation cost will thus be saved.

3. Multiscale thermomechanical topology optimization

In this section, proposed multiscale thermomechanical topology optimization is presented. A flow chart (Fig. 4) is shown to describe this approach. First, in terms of the force $\mathbf{f}$ and heat flux $\mathbf{f}_t$ applied to design domain Ω and surface Γ, a conceptual design having a density distribution $\boldsymbol{\theta}_c$ is generated, using macroscale thermo-mechanical topology optimization with a linear material interpolation. Elemental strains $\boldsymbol{\varepsilon}_1 \cdots \boldsymbol{\varepsilon}_{nel}$ and relative densities $\theta_1 \cdots \theta_{nel}$ of this conceptual design are evaluated. Based on these information, each unit cell is optimized through RVE-based inverse homogenization. Then, homogenized tensor $\left(\mathbf{D}^H_{C,1} \cdots \mathbf{D}^H_{C,nel}, \kappa^H_{C,1} \cdots \kappa^H_{C,nel}\right)$ and local stiffness matrix $\left(\mathbf{K}^H_1 \cdots \mathbf{K}^H_{nel}, \mathbf{K}^H_{t,1} \cdots \mathbf{K}^H_{t,nel}\right)$ of each optimal unit cells are computed through asymptotic homogenization (AH). With assembled global stiffness matrix $\left(\Sigma\mathbf{K}^H, \Sigma\mathbf{K}^H_t\right)$, the macroscale thermomechanical finite element analysis is performed to re-evaluated the objective. After these steps, the first iteration of multiscale optimization is finished. Since in the conceptual design, the linear interpolation represents a stiffer property than the actual material with same densities, the internal energy or compliance of resulting porous structure from the first iteration would be underestimated. Hence, design variables are updated by enabling additional mass and next iteration is performed. The approach contains three key concepts, namely macroscale structural design, mesoscale material design, and design updating scheme, which will be described in following sections.

3.1. Macroscale structure design

The purpose of marcoscale optimization is to use given mass, minimize the internal energy or compliance arising from external load $\mathbf{f}^\intercal\mathbf{u}$ and thermal expansion $\mathbf{f}_{th}{}^\intercal\mathbf{u}$, while remaining thermal compliance $\mathbf{f}_t{}^\intercal\mathbf{T}$ that adopted as a measurement of heat conduction, employed as a constraint. The constraint aims to use relax factor C_Q to define an upper bound of thermal compliance, in order to ensure a small thermal compliance which indicating high thermal performance. Additionally, In the optimization process, Hooke's and Fourier's law are served as physics constraints. Finally, macroscale thermomechanical

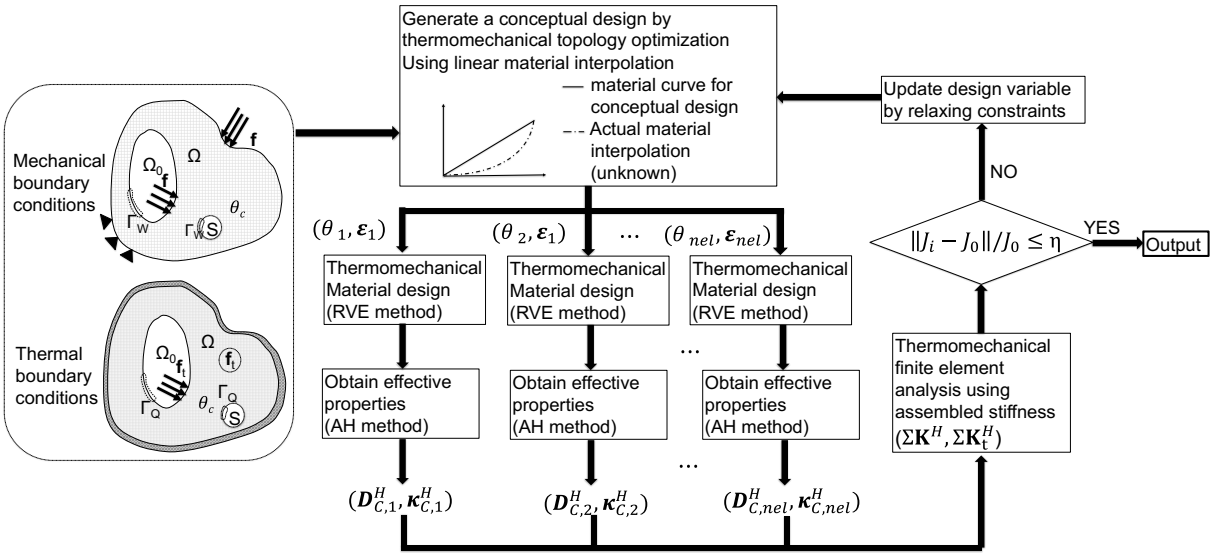

Figure 4: Flow chart of multiscale thermomechanical topology optimization.

topology optimization is stated as

$$\begin{aligned}
\text{given} \quad & m(\boldsymbol{\theta}_1) \\
\text{minimize} \quad & \mathbf{f}^\intercal \mathbf{u}(\boldsymbol{\theta}_1) + \mathbf{f}_{th}(\mathbf{T})^\intercal \mathbf{u}(\boldsymbol{\theta}_1) \\
\text{subject to} \quad & \mathbf{f}_t{}^\intercal \mathbf{T}(\boldsymbol{\theta}_1) \leq C_Q \mathbf{f}_t{}^\intercal \mathbf{T}(\boldsymbol{\theta}_0) \\
& m(\boldsymbol{\theta}_{\min}) \leq m(\boldsymbol{\theta}_1) \leq m(\boldsymbol{\theta}_0) \\
& \boldsymbol{\theta}^{\min} \leq \boldsymbol{\theta}_1 \leq \mathbf{1} \\
\text{satisfying} \quad & \mathbf{K}(\boldsymbol{\theta}_1)\mathbf{u}(\boldsymbol{\theta}_1) = \mathbf{f} + \mathbf{f}_{th} \\
& \mathbf{K}_t(\boldsymbol{\theta}_1)\mathbf{f}_t = \mathbf{T}(\boldsymbol{\theta}_1),
\end{aligned} \tag{10}$$

where $\boldsymbol{\theta}_1$ represents relative density distribution and $\boldsymbol{\theta}_0$ is the initial design; m is mass of macroscale structure; $\mathbf{f}$ is mechanical load and $\mathbf{f}_{th}$ is thermal expansion load; $\mathbf{u}$ is nodal displacement vector; $\mathbf{f}_t$ represents nodal heat flux and $\mathbf{T}$ nodal temperature. $\mathbf{K}$ is global stiffness matrix for mechanical; $\mathbf{K}_t$ is global stiffness for heat conduction. The sensitivity analysis of a coupled thermomechanical topology optimization is described in [24]. To analysis sensitivity of this problem, Eq. (10) can be rewritten as the form of Lagrangian function L:

$$\begin{aligned}
\text{find} \quad & \boldsymbol{\theta}_1^* \in \mathbb{R}^{n_c} \\
\text{minimize} \quad & L(\boldsymbol{\theta}_1) = (\mathbf{f} + \mathbf{f}_{th})^\intercal \mathbf{u}(\boldsymbol{\theta}_1) + \omega \mathbf{f}_t{}^\intercal \mathbf{T}(\boldsymbol{\theta}_1) \\
& \boldsymbol{\lambda}_m{}^\intercal (\mathbf{K}(\boldsymbol{\theta}_1)\mathbf{u}(\boldsymbol{\theta}_1) - \mathbf{f} - \mathbf{f}_{th}) + \boldsymbol{\lambda}_t{}^\intercal (\mathbf{K}_t(\boldsymbol{\theta}_1)\mathbf{T}(\boldsymbol{\theta}_1) - \mathbf{f}_t) \\
\text{subject to} \quad & m(\boldsymbol{\theta}_{\min}) \leq m(\boldsymbol{\theta}_1) \leq m(\boldsymbol{\theta}_0) \\
& \theta^{\min} \leq \theta_1 \leq 1,
\end{aligned} \tag{11}$$

where ω is a weighting factor, $\boldsymbol{\lambda_m}$ and $\boldsymbol{\lambda_t}$ are adjoint vectors. Notably, here the design dependent load $\mathbf{f}_{th}$ is not only a function of relative density $\boldsymbol{\theta}_1$, but also a function of temperature $\mathbf{T}$. Indeed, $\mathbf{T}$ is a function of $\boldsymbol{\theta}_1$. Thus, by using chain rule, the derivatives of the Lagrangian for each element θ_c are written as

$$\begin{aligned}
\frac{\partial L(\boldsymbol{\theta}_1)}{\partial \theta_c} =& \mathbf{u}(\boldsymbol{\theta}_1)^\intercal \frac{\partial \mathbf{f}_{th}}{\partial \theta_c} + \mathbf{u}(\boldsymbol{\theta}_1)^\intercal \frac{\partial \mathbf{f}_{th}}{\partial \mathbf{T}(\theta_1)} \frac{\partial \mathbf{T}(\theta_1)}{\partial \theta_c} + (\mathbf{f} + \mathbf{f}_{th})^\intercal \frac{\partial \mathbf{u}(\boldsymbol{\theta}_1)}{\partial \theta_c} + \omega \mathbf{f}_t{}^\intercal \frac{\partial \mathbf{T}(\boldsymbol{\theta}_1)}{\partial \theta_c} + \\
& \boldsymbol{\lambda}_m{}^\intercal \left(\frac{\partial \mathbf{K}(\theta_1)}{\partial \theta_c} \mathbf{u}(\boldsymbol{\theta}_1) + \mathbf{K}(\boldsymbol{\theta}_1) \frac{\partial \mathbf{u}(\boldsymbol{\theta}_1)}{\partial \theta_c} - \frac{\partial \mathbf{f}_{th}}{\partial \theta_c} - \frac{\partial \mathbf{f}_{th}}{\partial \mathbf{T}(\theta_1)} \frac{\partial \mathbf{T}(\boldsymbol{\theta}_1)}{\partial (\theta_c)} \right) + \\
& \boldsymbol{\lambda}_t{}^\intercal \left(\frac{\partial \mathbf{K}_t(\theta_1)}{\partial \theta_c} \mathbf{T}(\boldsymbol{\theta}_1) + \mathbf{K}_t(\boldsymbol{\theta}_1) \frac{\partial \mathbf{T}(\boldsymbol{\theta}_1)}{\partial \theta_c} \right)
\end{aligned} \tag{12}$$

where $\boldsymbol{\lambda}_m{}^\intercal$ and $\boldsymbol{\lambda}_t{}^\intercal$ are the vectors of adjoint variables. In order to cancel $\frac{\partial \mathbf{u}(\boldsymbol{\theta}_1)}{\partial \theta_c}$term and $\frac{\partial \mathbf{T}(\boldsymbol{\theta}_1)}{\partial \theta_c}$, the

value in adjoint vectors can be defined to satisfy

$$\begin{aligned}&((\mathbf{f}+\mathbf{f}_{th})^{\intercal}+\boldsymbol{\lambda}_m{}^{\intercal}\mathbf{K}(\boldsymbol{\theta}_1))\,\frac{\partial\mathbf{u}(\boldsymbol{\theta}_1)}{\partial\theta_c}=\mathbf{0}\\&\left(\mathbf{u}(\boldsymbol{\theta}_1)^{\intercal}\frac{\partial\mathbf{f}_{th}}{\partial\mathbf{T}(\theta_1)}+\boldsymbol{\lambda}_t{}^{\intercal}\mathbf{K}_t(\boldsymbol{\theta}_1)-\boldsymbol{\lambda}_m{}^{\intercal}\frac{\partial\mathbf{f}_{th}}{\partial\mathbf{T}(\theta_1)}+\omega\mathbf{f}_t{}^{\intercal}\right)\frac{\partial\mathbf{T}(\boldsymbol{\theta}_1)}{\partial\theta_c}=\mathbf{0},\end{aligned}\tag{13}$$

where

$$\frac{\partial\mathbf{f}_{th}}{\partial\mathbf{T}(\theta_1)}=\mathbf{K}_{mt}(\boldsymbol{\theta}_1),\tag{14}$$

where $\mathbf{K}_{mt}$ is the thermo-mechanical coupling matrix. By sequentially solving the above two equations, finally, the sensitivity is derived as

$$\frac{\partial L(\boldsymbol{\theta}_1)}{\partial\theta_c}=\mathbf{u}(\boldsymbol{\theta}_1)^{\intercal}\frac{\partial\mathbf{f}_{th}}{\partial\theta_c}+\boldsymbol{\lambda}_m{}^{\intercal}\left(\frac{\partial\mathbf{K}(\theta_1)}{\partial\theta_c}\mathbf{u}(\boldsymbol{\theta}_1)-\frac{\partial\mathbf{f}_{th}}{\partial\theta_c}\right)+\boldsymbol{\lambda}_t{}^{\intercal}\frac{\partial\mathbf{K}_t(\theta_1)}{\partial\theta_c}\mathbf{T}(\boldsymbol{\theta}_1)\tag{15}$$

In proposed multiscale approach, macroscale topology optimization is only called one time to generate a conceptual design. The design is generated using linear material interpolation, method of moving asymptotes (MMA) solver [25] and no filters.

3.2. Mesoscale material design

By using the information provided by macroscale conceptual design, maximum bulk modulus, shear modulus and heat conduction for each unit cell can be found through RVE-based inverse homogenization method. With application of elemental relative density $m(\boldsymbol{\theta}_{ne})$, strain $\boldsymbol{\varepsilon}(\boldsymbol{\theta}_{ne})$ and temperature gradient $\nabla\mathbf{T}(\boldsymbol{\theta}_{ne})$ derived from macroscale conceptual optimization, an inverse homogenization is written as a minimum compliance problem. It is stated as a displacement based, multiple-load cases topology optimization:

$$\begin{aligned}\text{given}\quad&m(\boldsymbol{\theta}_{ne}),\boldsymbol{\varepsilon}(\boldsymbol{\theta}_{ne}),\nabla\mathbf{T}(\boldsymbol{\theta}_{ne})\\\text{minimize}\quad&\sum_{i=1}^{n}\mathbf{f}_i(\mathbf{u})^{\intercal}\mathbf{u}_i(m(\boldsymbol{\theta}_{ne}),\boldsymbol{\varepsilon}(\boldsymbol{\theta}_{ne}))\quad\text{or}\quad\sum_{i=1}^{n}\mathbf{f}_{t,i}(\nabla\mathbf{T})^{\intercal}\mathbf{T}_i(m(\boldsymbol{\theta}_{ne}),\nabla\mathbf{T}(\theta_{ne}))\\\text{subject to}\quad&m(\boldsymbol{\theta}_{\min})\le m(\boldsymbol{\theta})\le m(\boldsymbol{\theta}_{ne})\\&\boldsymbol{\theta}^{\min}\le\boldsymbol{\theta}\le\boldsymbol{\theta}^{\max}\\\text{satisfying}\quad&\mathbf{K}(\boldsymbol{\theta}_{ne})^{-1}\mathbf{u}(\boldsymbol{\theta}_{ne})=\mathbf{f}\\&\mathbf{K}_t(\boldsymbol{\theta}_{ne})^{-1}\mathbf{T}(\boldsymbol{\theta}_{ne})=\mathbf{f}_t,\end{aligned}\tag{16}$$

where mechanical compliance (extreme elasticity property) or thermal compliance (extreme heat conduction) for each unit cell is stated as an objective. n is the number of load cases. For a 2D RVE, $n=2$, and for a 3D RVE, $n=6$. The loads in each load case are induced by prescribed displacement or temperature gradient, which are defined in Fig. 5 for a 2D RVE.

The inverse homogenization problems for 2D RVEs are solved using in-house Matlab code, in which solid isotropic material penalization (SIMP) method [26] , MMA solver and density based filter are used. Fig. 6 shows resulting topologies using given relative density $m(\boldsymbol{\theta}_{ne})$=0.19, 0.5 and 0.81, prescribed strain $\boldsymbol{\varepsilon}(\boldsymbol{\theta}_{ne})=(1,1,1)$, and prescribed temperature gradient $\nabla\kappa(\boldsymbol{\theta}_{ne})=(1,1)$. Each unit cell is composed of 80×80 elements, but only a quarter of the structure (40×40 elements) is required to be analyzed. The results are consistent with reference ([27, 28, 20]). 3D extension is developed based on Top3d program [29]. Similarly, the optimum topologies are obtained using SIMP method, MMA solver and density based filter with $m(\boldsymbol{\theta}_{ne})$=0.259, 0.5 and 0.74, prescribed strain $\boldsymbol{\varepsilon}(\boldsymbol{\theta}_{ne})=(1,1,1,1,1,1)$, and prescribed temperature gradient $\nabla\kappa(\boldsymbol{\theta}_{ne})=(1,1,1)$ (Fig. 7). The results are shown as a distribution of $2\times2\times2$ unit cells to illustrate the connectivity. Each unit cell is composed of $(40\times40\times40)$ elements, but only 1/8 of the structure $(20\times20\times20)$ is required to be analyzed. To facilitate the removal of extra material cost in AM process, open channels are defined as passive elements, making $m(\boldsymbol{\theta}_{\max})$=0.8.

As mentioned in the introduction, among the optimum topologies in Fig. 6 and Fig. 7, for the unit cells having maximum shear modulus (the first row), the angle between each tilt bar and horizontal

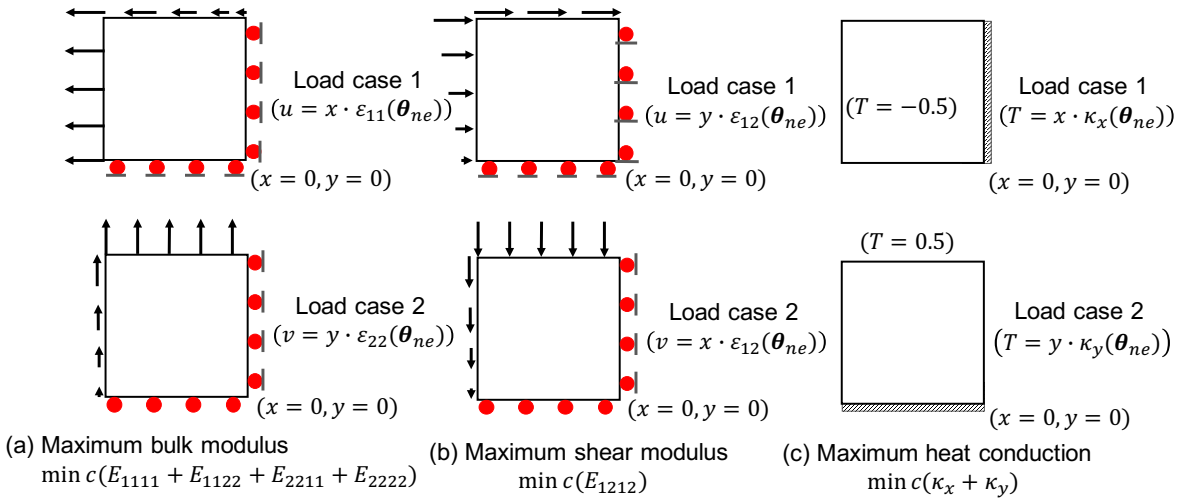

Figure 5: Prescribed displacement (or temperature gradient) and supports (or insulated boundary) for the purpose of maximizing extreme properties.

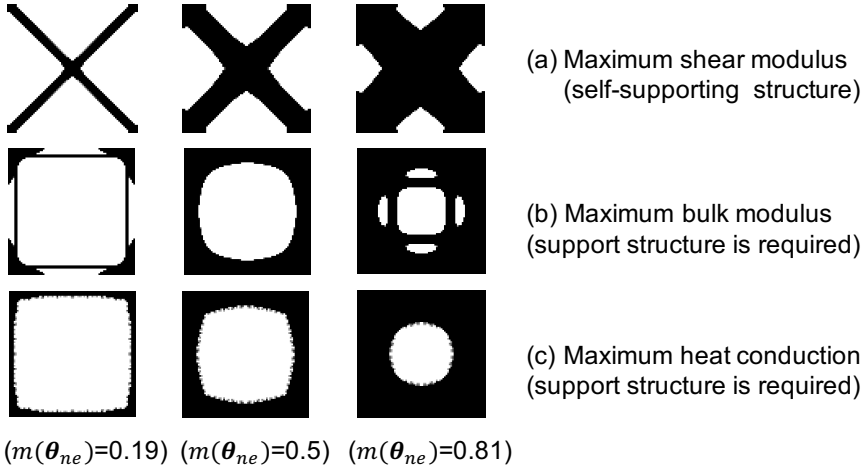

Figure 6: 2D results from RVE-based inverse homogenization.

plane is approximately 45°, obtaining a self-supporting structure. Compared to them, those unit cells having maximum bulk modulus and heat conduction contain overhangs that required additional support materials. In terms of maintaining a self-supporting structure, maximum shear modulus is a preferred objective function in material design. Notably, this objective function may not guarantee the overall material's thermo-mechanical properties, which will be achieved through design updating.

3.3. Updating rule of multiscale design

After macroscale topology optimization and mesoscale material design for each unit cell, one iteration is finished. Next, the homogenized properties of each unit cell are evaluated through asymptotic homogenization. Then global stiffness matrices are assembled and a new macroscale objective value can be evaluated by calling thermomechanical finite element analysis. This value may be a suboptimal value compared to conceptual design for two reasons: First, the material interpolation used in conceptual design is stiffer hence the thermomechanical performance would be overestimated; Second, the objective function in the material design is maximizing shear modulus, which may not ensure the overall optimality of thermo-mechanical performance for each unit cell. A design update scheme is therefore required to

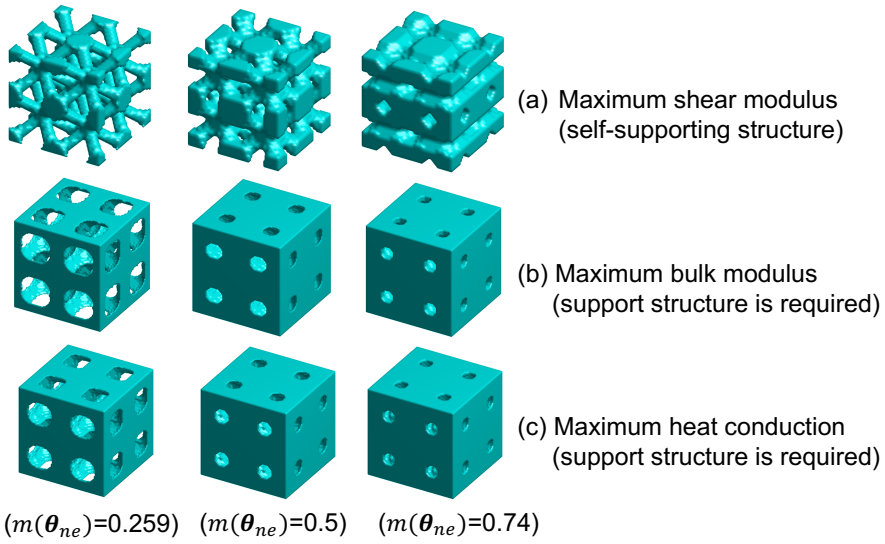

Figure 7: 3D results from RVE-based inverse homogenization.

revise the suboptimal macroscale objective value close to the anticipated value:

$$\eta_i = \| J_i - J_0 \| / J_0 \leq \eta, \tag{17}$$

where J_i is the objective evaluation of ith iteration, J_0 is objective of conceptual design, η is a small number. The following Hybrid Cellular Automata (HCA) [30] principle is employed to update elemental design variable x_i or its Moore neighborhood $\mathcal{N}_{\mathcal{M}}$, based on local objective value:

$$\begin{aligned}
\text{if} \quad & J_{i,ne} \geq J_{0,ne} \quad \text{and} \quad x_{i,ne} \leq x_{\max}, \quad x_{i+1,ne} = x_{i,ne} + \delta \\
\text{elseif} \quad & J_{i,ne} \leq J_{0,ne} \quad \text{and} \quad x_{i,ne} \geq x_{\min}, \quad x_{i+1,ne} = x_{i,ne} - \delta \\
\text{elseif} \quad & J_{i,ne} \geq J_{0,ne} \quad \text{and} \quad x_{i,ne} = x_{\max}, \quad x_{i+1,\mathcal{N}_{\mathcal{M}}} = x_{i,\mathcal{N}_{\mathcal{M}}} + \delta \\
\text{elseif} \quad & J_{i,ne} \leq J_{0,ne} \quad \text{and} \quad x_{i,ne} = x_{\min}, \quad x_{i+1,\mathcal{N}_{\mathcal{M}}} = x_{i,\mathcal{N}_{\mathcal{M}}} - \delta
\end{aligned} \tag{18}$$

These updated design variables are adopted to material design in next iteration.

3.4. Two dimensional numerical example

A 2D example is presented to illustrate the proposed multiscale approach. A $3cm \times 1cm$ MBB beam is meshed by 15×5 square voxels (Fig. 8). A downward mechanical load $F = 1N$ is located at the top left corner, and the fixed constraint is located at the bottom right corner. Meanwhile, a point-wise heat flux $q = 1W$ is located at the top left corner, and a boundary temperature $T = 0°C$ is located at the bottom right corner. The specified material is 420 stainless steel infiltrated with bronze, having density $7.86g/cm^3$, Young's stiffness $E = 147GPa$, heat conductivity $k = 22.6W/m \cdot K$, thermal expansion coefficient $\alpha = 7.4 \times 10^{-6}K^{-1}$. Assume in the conceptual design, the objective is minimizing the compliance due to the thermo-mechanical load within 50% volume fraction. The minimum relative density for each unit cell is $m(\boldsymbol{\theta}_{ne}) = 0.19$. The coefficient of thermal performance C_Q is equal to 3. The resulting topology is shown in Fig. 8 (a), having a normalized compliance equal to 1. Then in mesoscale, the shear modulus of each unit cell in this 15×5 frame is optimized based on the strain and relative density information derived from conceptual design.

After the first iteration, the topology of the MBB beam is shown as Fig. 8 (b). The homogenized properties of this structure is assembled to re-estimate the actual compliance and strain information via thermo-mechanical finite element analysis. In this example, the re-estimate compliance is about 61.4 % greater than the conceptual design. Thus the design updating allows unit cells having local compliance greater than conceptual design to add material, while in the unit cell having smaller local compliance compared to conceptual design, material would be partly removed. The material adding and removal rate δ is defined as

$$\delta = 0.05 \times \eta_i, \tag{19}$$

where $\eta_i = 0.05$. Based on the updated strain and relative density information, the topology of each unit cell is optimized in the second iteration. This iterative process is repeated 28 times before the convergence criteria satisfied. The final volume fraction to achieve the expected compliance is 65.5 %. The total computation time is 741.9 seconds, using Matlab in a Macbook Pro computer having 3.1 GHZ Intel Core i7 and 16 GB MHZ DDR3 memory.

Table 1: Comparison between the solid MBB beam, optimized porous MBB beam and the uniform porous MBB beam.

	Weight (g)	Max Von Mises stress (MPa)	Max temperature (°C)
Solid MBB beam	2.358	1.840	102.2
Optimized porous MBB beam	1.179	2.417	190.8
Uniform porous MBB beam	1.179	4.932	213.4

Finally, the optimal design is converted to a solid file with 0.1cm thickness, and verified by thermo-mechanical finite element simulation using COMSOL Multiphysics. The results of stress and temperature fields are compared to the simulation results of a uniform porous MBB beam having the same volume fraction, as well as a solid MBB beam (Fig. 9 and Table 1). It indicates that, an optimal porous structure, although compromising stiffness and heat transfer capability with respect to a solid counterpart, significantly improves thermo-mechanical performance compared to a uniform porous MBB beam with the same volume fraction.

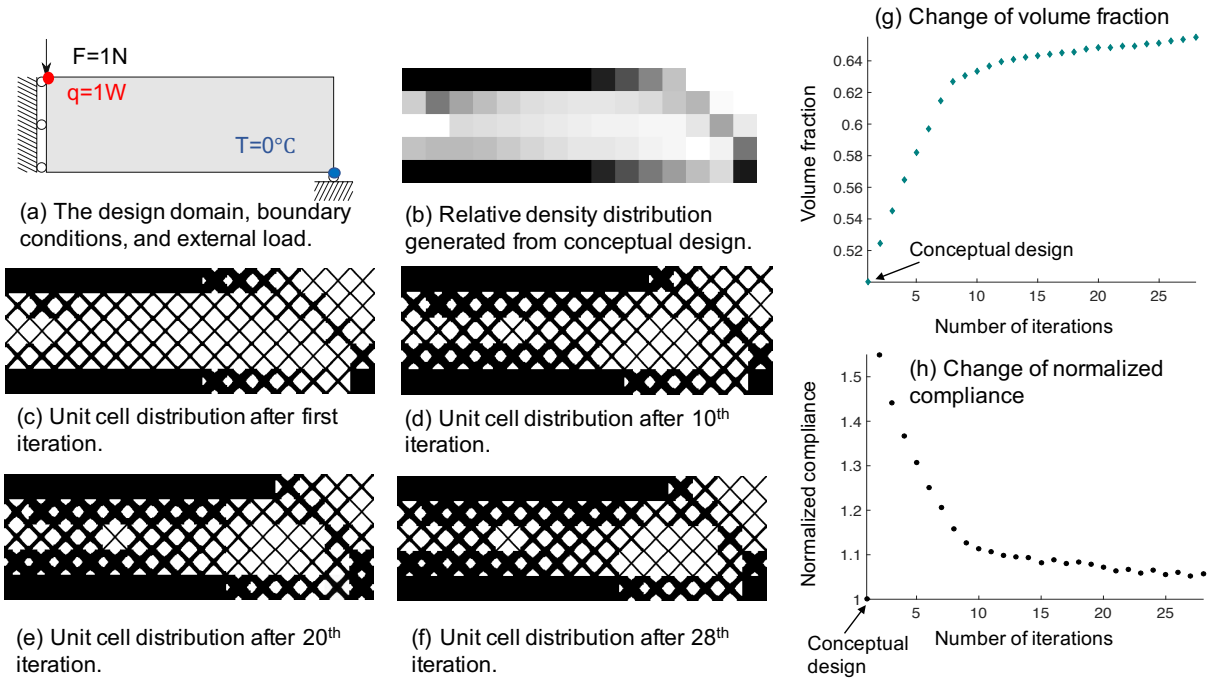

Figure 8: A 2D MBB beam example presented to illustrate the proposed algorithm.

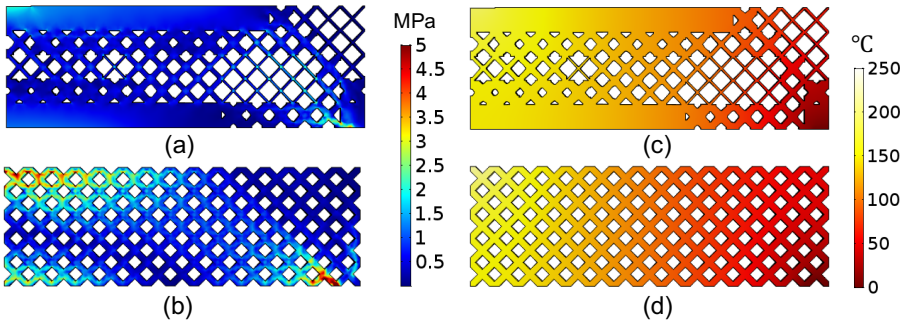

Figure 9: Thermo-mechanical simulation of the optimized result ((a) stress field, and (c) temperature field), as well as the simulation results of a uniform MMB beam having same volume fraction ((b) stress field, and (d) temperature field).

4. Application to porous injection mold

A 3D porous injection mold design is presented in this section. The mold is a 3 in $\times$ 3 in $\times$ 1.25 in core insert. Based on the geometry of the mold, a quarter of mold section is investigated. Besides, the top core of the mold is reserved as solid structure for conformal cooling design (Fig. 10 (a) to (e)). Injection load located at the injected part surface, clamping pressure at imposed on bottom, and press-fit load on lateral sides are served as mechanical force. For heat conduction, a heat flux imposed on the injected part surface, and the temperature of cooling pipe is assumed as a constant value. All physics values are normalized in this problem.

In the problem statement, define given macroscale mass fraction $m(\theta)$=0.5, C_Q=1.1, η=0.2, $\delta = 0.05 \times \eta_i$. A $6 \times 6 \times 5$ cubic mesh is applied to the macroscale problem, while a $20 \times 20 \times 20$ cubic mesh is used for each of mesoscale voxel. However, in mesoscale, only 1/8 of each cubic is required to analyze. The convergence is satisfied after 15 iteration with $m(\boldsymbol{\theta})$=0.71 (Fig. 10 (f) and (g)). The total computation time is 61652 seconds (17.4 hours), using Matlab in a Macbook Pro computer having 3.1 GHZ Intel Core i7 and 16 GB MHZ DDR3 memory.

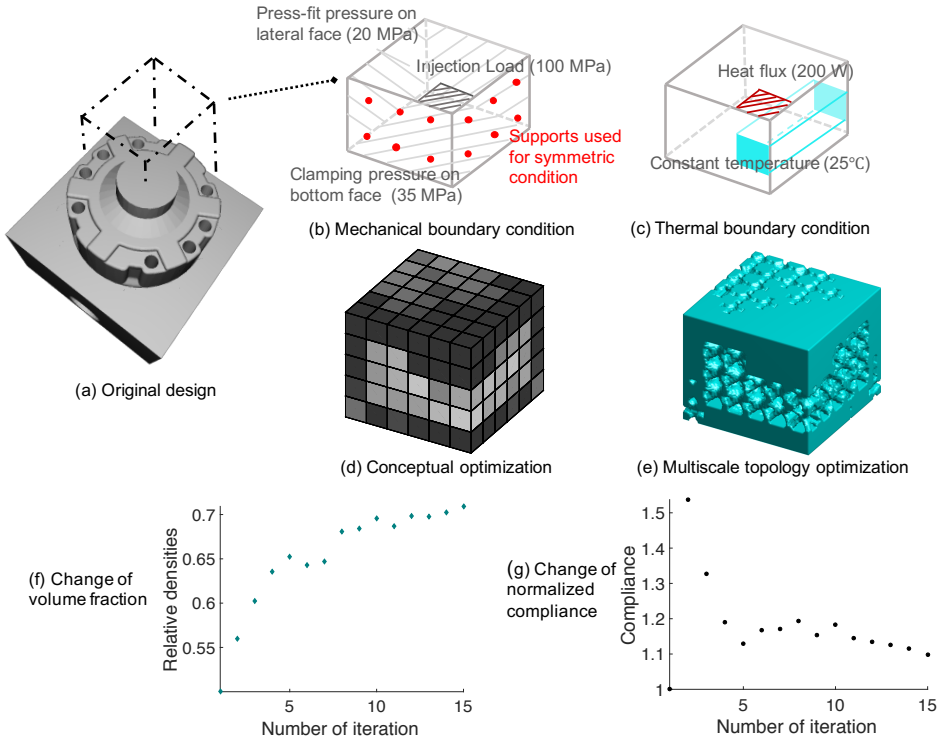

Figure 10: Multiscale thermomechanical topology optimization of a porous injection mold.

Finally, the optimal design is remeshed using 3-Matics and verified by thermo-mechanical finite element simulation using COMSOL Multiphysics. The results of stress field and temperature are compared to the simulation results of a uniform porous mold having the same volume fraction, as well as a solid mold (Fig. 11 and Table 2). It indicates that, unlike a uniform porous mold having the same volume fraction, though the weight of the optimal porous mold is 29% lighter than the solid counterpart, the maximum Von Mises stress is below the yield strength of the material (427 MPa), and the maximum temperature in the mold doesn't have a significant change.

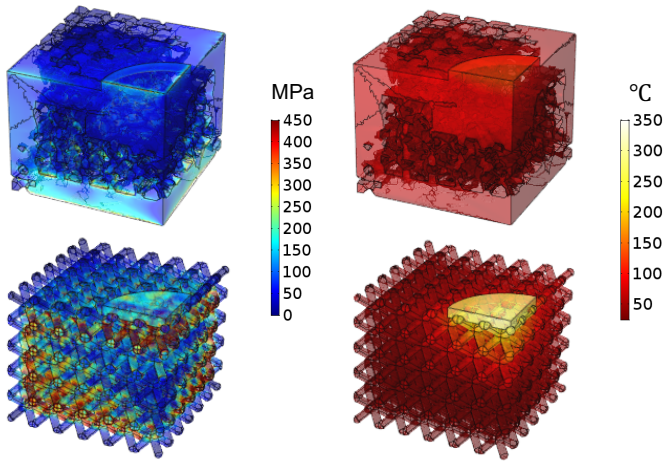

Figure 11: Thermo-mechanical simulation of the optimized result ((a) stress field, and (c) temperature field), as well as the simulation results of a uniform MMB beam having same volume fraction ((b) stress field, and (d) temperature field).

Table 2: Comparison between the solid mold, optimized porous mold and the uniform porous mold.

	Weight (kg)	Max Von Mises stress (MPa)	Max temperature (°C)
Solid mold	2.095	280.3	126.9
Optimized porous mold	1.487	325.5	127.1
Uniform porous mold	1.487	720.7	312.3

The optimal structure is approximated to an iso-surface and meshed to a STL file. The file size is 125.7Mb, composed of 2511164 triangles. After modification in Netfabb, the triangle number is reduced to 374558, with a limit of deformation 0.01 in.

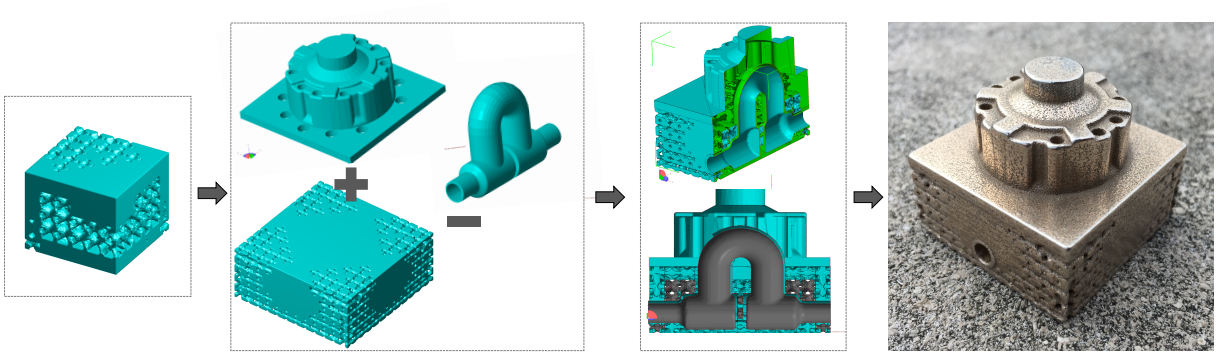

Figure 12: Assemble and prototyping process of the injection mold.

5. Additive manufacturing and planning of experimental test

After mirroring the resulting section and performing Boolean operations to assemble the top core and conformal cooling channel, the porous injection mold is prototyped using Direct Metal Laser sintering (DMLS), with a scale factor 0.4 (Fig. 12). The scaled prototype was fabricated by an additive manufacturing service company (Shapeways, Newyork, U.S.). The printed steel is Stainless Steel Alloy 420 infiltrated with Bronze (90 %Cu / 10 % Sn). It is a matrix material composed of 60 % stainless steel and 40% bronze. The minimum wall thickness of this protocol is 1.0 mm, and the maximum length of hole allowing the materials to be removed is 2.0 mm. This scaled down prototype proves the internal lattice structure is self-supporting without the requirement to change the orientation of the mold. In the near future, the original size of the injection mold will be manufactured and experimental test will be employed. Before that, samples will be generated using the same machine and material, and experimental tests are planned to validate the mechanical and thermal properties (Fig. 13). These samples, composed of solid and porous materials, are designed based on ASTM E8, ASTM E9 and ASTM E1530 standards for the tensile, compression and thermal conductivity experiments, respectively. The experimental properties such as Young's modulus, Poisson's ratio, yield strength and thermal conductivity will be incorporated into the aforementioned examples to improve the accuracy of the solution.

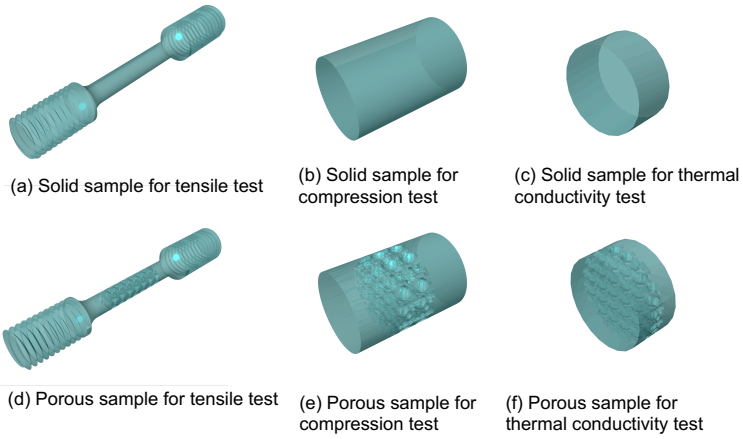

Figure 13: Experimental samples to validate the thermal and mechanical properties.

6. Conclusion

An innovative multiscale thermo-mechanical topology optimization method has been presented for generating injection molds. Compared to traditional studies, the proposed method is computationally efficient, and amiable to additive manufacturing by consisting of self-supporting lattice/porous structures. The thermo-mechanical performance of the injection mold is maximized with given volume fraction, and the self-supporting unit cells are formed by maximizing shear modulus with taking account of local relative densities and strains. The design is updated after comparing local objective value and the desired value after each iteration until the thermo-mechanical performance of the mold is satisfied. The proposed design method is proved through the optimization of a solid mold insert. The optimized porous injection mold is about 30 % lighter than the solid counterpart, but the thermo-mechanical performance including Von Mises stress and surface temperature is approved. The resulting porous structure is tessellated in a stereolithography (STL) file. A scaled down physical prototype of the mold was fabricated using DMLS procedure without internal support structure to demonstrate the manufacturability of the optimal design.

Some limitations of this study should also be considered. First, since the macroscale design only provides a conceptual design by using a coarse mesh, the feasibility of the final design is required to be verified by simulation of entire structure involving both scales, or by experiments. In addition, the assembling process often requires a reduction of surface mesh to adapt the computer memory, which will slightly change the lattices' shape and compromise the accuracy. Furthermore, post processing CAD software such as Netfabb is still required in combination with the proposed algorithm, to assemble porous structure with mold pipes, ejector pins, injection gate, bolts and other detail geometries, which may require high computer memory (more than 12GB RAM). In the future work, a more efficient assembling method is worth to investigate. Furthermore, the field testing for the optimized design will be implemented, in

order to collect the experimental data and improve the design method.

7. Acknowledgements

The Walmart Foundation supported this research effort. Hewitt Molding Company provided the original injection mold model for the investigation. Any opinions, findings, conclusions, and recommendations expressed in this investigation are those of the writers and do not necessarily reflect the views of the sponsors.

References

[1] David O Kazmer. *Injection mold design engineering*. Carl Hanser Verlag GmbH Co KG, 2016.

[2] Lars-Erik Rännar, Anders Glad, and Claes-Göran Gustafson. Efficient cooling with tool inserts manufactured by electron beam melting. *Rapid Prototyping Journal*, 13(3):128–135, 2007.

[3] Yunlong Tang and Yaoyao Fiona Zhao. A survey of the design methods for additive manufacturing to improve functional performance. *Rapid Prototyping Journal*, 22(3):569–590, 2016.

[4] Gabriel Antonio Mendible, Jack A Rulander, and Stephen P Johnston. Comparative study of rapid and conventional tooling for plastics injection molding. *Rapid Prototyping Journal*, 23(2):344–352, 2017.

[5] Tomas Zegard and Glaucio H. Paulino. Bridging topology optimization and additive manufacturing. *Structural and Multidisciplinary Optimization*, 2015.

[6] Jikai Liu and Yongsheng Ma. A survey of manufacturing oriented topology optimization methods. *Advances in Engineering Software*, 100:161–175, 2016.

[7] E.M. Dede. Optimization and design of a multipass branching microchannel heat sink for electronics cooling. *Journal of Electronic Packaging*, 134(4):041001 (10 pp.), 2012.

[8] Tong Wu, Suchana A Jahan, Praveen Kumaar, Andres Tovar, Hazim El-Mounayri, Yi Zhang, Jing Zhang, Doug Acheson, Kim Brand, and Razi Nalim. A framework for optimizing the design of injection molds with conformal cooling for additive manufacturing. *Procedia Manufacturing*, 1:404–415, 2015.

[9] H Rodrigues, Jose M Guedes, and MP Bendsoe. Hierarchical optimization of material and structure. *Structural and Multidisciplinary Optimization*, 24(1):1–10, 2002.

[10] Jiadong Deng, Jun Yan, and Gengdong Cheng. Multi-objective concurrent topology optimization of thermoelastic structures composed of homogeneous porous material. *Structural and Multidisciplinary Optimization*, pages 1 – 15, 2012.

[11] Jiadong Deng, Jun Yan, and Gengdong Cheng. Multi-objective concurrent topology optimization of thermoelastic structures composed of homogeneous porous material. *Structural and Multidisciplinary Optimization*, 47(4):583–597, 2013.

[12] Liang Xia. *Multiscale structural topology optimization*. Elsevier, 2016.

[13] Sajad Arabnejad Khanoki and Damiano Pasini. Multiscale design and multiobjective optimization of orthopedic hip implants with functionally graded cellular material. *Journal of biomechanical engineering*, 134(3):031004, 2012.

[14] Pu Zhang, Jakub Toman, Yiqi Yu, Emre Biyikli, Mesut Kirca, Markus Chmielus, and Albert C To. Efficient design-optimization of variable-density hexagonal cellular structure by additive manufacturing: Theory and validation. *Journal of Manufacturing Science and Engineering*, 137(2):021004, 2015.

[15] Tong Wu, Kai Liu, and Andres Tovar. Multiphase topology optimization of lattice injection molds. *Computers & Structures*, 192:71–82, 2017.

[16] Ahmed Hussein, Liang Hao, Chunze Yan, Richard Everson, and Philippe Young. Advanced lattice support structures for metal additive manufacturing. *Journal of Materials Processing Technology*, 213(7):1019–1026, 2013.

[17] F Calignano. Design optimization of supports for overhanging structures in aluminum and titanium alloys by selective laser melting. *Materials & Design*, 64:203–213, 2014.

[18] Xiaojian Wang, Shanqing Xu, Shiwei Zhou, Wei Xu, Martin Leary, Peter Choong, M Qian, Milan Brandt, and Yi Min Xie. Topological design and additive manufacturing of porous metals for bone scaffolds and orthopaedic implants: a review. *Biomaterials*, 83:127–141, 2016.

[19] X Huang, A Radman, and YM Xie. Topological design of microstructures of cellular materials for maximum bulk or shear modulus. *Computational Materials Science*, 50(6):1861–1870, 2011.

[20] Shiwei Zhou, Joseph Cadman, Yuhang Chen, Wei Li, Yi Min Xie, Xiaodong Huang, Richard Appleyard, Guangyong Sun, and Qing Li. Design and fabrication of biphasic cellular materials with transport properties–a modified bidirectional evolutionary structural optimization procedure and matlab program. *International Journal of Heat and Mass Transfer*, 55(25):8149–8162, 2012.

[21] Ole Sigmund. Materials with prescribed constitutive parameters: an inverse homogenization problem. *International Journal of Solids and Structures*, 31(17):2313–2329, 1994.

[22] Liang Xia and Piotr Breitkopf. Design of materials using topology optimization and energy-based homogenization approach in matlab. *Structural and multidisciplinary optimization*, 52(6):1229–1241, 2015.

[23] Erik Andreassen and Casper Schousboe Andreasen. How to determine composite material properties using numerical homogenization. *Computational Materials Science*, 83:488–495, 2014.

[24] O. Sigmund. Design of multiphysics actuators using topology optimization. i. one-material structures. *Computer Methods in Applied Mechanics and Engineering*, 190(49-50):6577 – 604, 2001/10/12.

[25] Krister Svanberg. The method of moving asymptotesa new method for structural optimization. *International journal for numerical methods in engineering*, 24(2):359–373, 1987.

[26] Martin P Bendsøe, Ole Sigmund, Martin P Bendsøe, and Ole Sigmund. *Topology optimization by distribution of isotropic material*. Springer, 2004.

[27] Ole Sigmund. A new class of extremal composites. *Journal of the Mechanics and Physics of Solids*, 48(2):397–428, 2000.

[28] MM Neves, H Rodrigues, and J Miranda Guedes. Optimal design of periodic linear elastic microstructures. *Computers & Structures*, 76(1):421–429, 2000.

[29] Kai Liu and Andrés Tovar. An efficient 3d topology optimization code written in matlab. *Structural and Multidisciplinary Optimization*, 50(6):1175–1196, 2014.

[30] Charles L Penninger, Neal M Patel, Glen L Niebur, Andrés Tovar, and John E Renaud. A fully anisotropic hierarchical hybrid cellular automaton algorithm to simulate bone remodeling. *Mechanics Research Communications*, 35(1):32–42, 2008.